CCFE-PR(16)75

A. De Backer, A. E. Sand, K. Nordlund, L. Luneville, D. Simeone
and S. L. Dudarev

Sub-cascade formation and defect cluster size scaling in high-energy collision events in metals

Sub-cascade formation and defect cluster size scaling in high-energy collision events in metals

A. De Backer[1], A. E. Sand[2], K. Nordlund[2], L. Luneville[3;4], D. Simeone[4;5] and S. L. Dudarev[1]

[1] CCFE, Culham Science Centre, Abingdon, Oxon OX14 3DB, United Kingdom
[2] Department of Physics, University of Helsinki - P.O. Box 43, FI-00014 Helsinki, Finland
[3] CEA/DANS/DMN/SERMA/LLPR-LRC CARMEN, CEA Saclay 91191 Gif sur Yvette, France
[4] Centralesupelec/SPMS/LRC CARMEN, 92292 Chatenay Malabry, France
[5] CEA/DANS/DMN/SRMA/LA2M-LRC CARMEN, CEA Saclay 91191 Gif sur Yvette, France

Sub-cascade formation and defect cluster size scaling in high-energy collision events in metals

A. De Backer[1], A. E. Sand[2], K. Nordlund[2], L. Luneville[3,4], D. Simeone[4,5] and S. L. Dudarev[1]

[1] *CCFE, Culham Science Centre, Abingdon, Oxon OX14 3DB, United Kingdom*
[2] *Department of Physics, University of Helsinki - P.O. Box 43, FI-00014 Helsinki, Finland*
[3] *CEA/DANS/DMN/SERMA/LLPR-LRC CARMEN, CEA Saclay 91191 Gif sur Yvette, France*
[4] *Centralesupelec/SPMS/LRC CARMEN, 92292 Chatenay Malabry, France*
[5] *CEA/DANS/DMN/SRMA/LA2M-LRC CARMEN, CEA Saclay 91191 Gif sur Yvette, France*

PACS 61.80.Az – Theory and Models of Radiation Effects
PACS 61.82.Bg – Metals and Alloys
PACS 61.72.J- – Point Defects and Defect clusters

Abstract – A critical constraint associated with the application of defect production cluster size scaling laws established in recent studies [1, 2], to radiation phenomena occurring over a broad range of irradiation conditions, is the limitation on the energy of the incident particles at which the scaling laws still apply. Incident neutrons or ions, with energies exceeding a certain energy threshold, produce a complex hierarchy of collision sub-cascade events, which impedes the use of the defect cluster size scaling law derived for an individual low-energy cascade. By analyzing the statistics of sub-cascade sizes and energies, we show that defect clustering at super-threshold energies can be described by a convolution of two scaling laws, one for the energies of sub-cascades and the other for the sizes of defect clusters formed in sub-cascades. The statistics of sub-cascade sizes exhibits a transition at the threshold energy, where the sub-cascade morphology changes from a single molten domain below the threshold, to several or many molten sub-domains above the threshold. The number of sub-domains then increases in proportion to the energy of the primary knock-on atom. The model has been validated against direct molecular dynamics simulations and applied to W, Fe, Be, Zr and sixteen other metals, enabling the prediction of full statistics of defect cluster sizes with no limitation on the energy of a cascade event. We find that populations of defect clusters produced by the fragmented high-energy cascades are dominated by individual Frenkel pairs and small defect clusters, whereas the lower-energy non-fragmented cascades produce a greater proportion of large defect clusters.

Introduction. – Changes in physical and mechanical properties of materials, exposed to neutron and ion irradiation in nuclear reactors, fusion devices, or particle accelerators, occur as a result of generation of defects, their clustering, formation of dislocation loops and dislocations, and the subsequent evolution of radiation-induced microstructure driven by diffusion and interactions between the defects. In alloys, including those formed due to transmutation nuclear reactions [3], chemical segregation also occurs, resulting in the

formation of helium bubbles [4–6], chromium or rhenium precipitates [7, 8], and grain boundary embrittlement [9, 10]. Interpreting the observed microstructural evolution effects requires extending the measure of radiation damage beyond the *displacement per atom* (dpa) concept, proposed by Norgett *et al.* [11] to quantify the exposure of materials to fluxes of energetic particles [12].

Defining a physical measure of accumulation of defects in materials under collision cascade conditions involves recognizing the fact that clusters of defects form directly in collision cascade events [13, 14]. Sand *et al.* [1] and Yi *et al.* [2] showed that the statistics of defect cluster sizes formed in relatively low-energy cascades is well described by a power law distribution, similar to the power law describing the statistics of fragmentation of objects [15]. However, there remains an outstanding question that simulations and observations performed in Refs. [1, 2] did not address. The question concerns the role played by the fragmentation of cascades themselves. Such fragmentation occurs if the energy of a primary knock-on atom (PKA), initiating a cascade event, exceeds a certain threshold value. What remains unexplored is the effect of cascade fragmentation on the global statistics of defect clustering. In this Letter we investigate and resolve this question.

Cascade fragmentation is a phenomenon occurring if the energy of a PKA produced by an incident neutron [16] exceeds a threshold value, which is close to 30 keV in iron and 160 keV in tungsten. The fact that it is a high-energy phenomenon suggests that it can be reasonably well described by a treatment that neglects the many-body aspects of interatomic interactions involving valence electrons.

Molecular dynamics simulations of cascade fragmentation [17] show that the character of defect clusters formed in high energy cascade events does not change above the fragmentation threshold. On the other hand, the formation of sub-cascades may influence the defect cluster size distribution. The statistics of sub-cascade fragmentation was first investigated by Hou [18], who developed a fuzzy clustering method and applied it to the study of cascades in Au. Satoh *et al.* [19] proposed a model for cascade fragmentation and investigated high-energy cascades in Al, Cu and Au, exploring the dependence of cascade configurations on atomic number and density. Simeone *et al.* and Luneville *et al.* [20, 21] extended the work by Cheng *et al.* [22] and developed a fractal approach to the treatment of cascades. Heinisch and Singh [23] performed an extensive study of cascade fragmentation in several fcc, bcc, and hcp metals. Cascade fragmentation was found to correlate primarily with the atomic mass and charge. The threshold energy for cascade fragmentation was identified from the statistics of sub-cascades and distances between them. A recent example, illustrating the effect of cascade fragmentation on the resulting defect cluster size population, is provided by molecular dynamics simulations of very high energy cascades in Fe performed by Zarkadoula *et al.* [24]. Simulations show that populations of defects formed in 500 keV cascades are visibly dominated by individual Frenkel pairs and small defect clusters, with almost no large defect clusters present in the cascade debris. Our analysis, given below, explains this effect and generalizes it to a broad range of materials and irradiation conditions.

We use a binary collision approximation (BCA) model to investigate the spatial repartition of energy associated with the primary recoil and subsequent atomic collisions. The relative simplicity of the BCA model makes it possible to apply the treatment to almost any pure material or alloy, and to a broad range of incident particles - neutrons or ions - initiating the cascade events. Our treatment of cascade fragmentation is focused on the formation of molten sub-domains. This produces statistical information that can be combined with the data on defect formation during recrystallization, deduced from molecular dynamics (MD) simulations. Our method is different from earlier simulations by Broeders *at al.* [25] in that we take full cascade information into account and relate the effective molten volumes of sub-cascades to equivalent SKA secondary knock-on atom (SKA) energies, in this way mapping the statistics of molten volumes to the global distribution of defect cluster sizes associated with the entire cascade event.

Sub-domain decomposition combines the BCA treatment of a cascade with a model for

melting in a sub-domain. The cascade volume is then decomposed into elementary cubes (ECs), enabling the identification of distinct molten sub-domains. We apply the model to W and Fe and investigate the statistics of cascade events in these two materials, exploring the dependence of sub-domain distributions and molten volumes on the PKA energy, the choice of the EC size, and electronic energy losses. We analyze the dependence of cascade fragmentation on the atomic number and mass density of the material in twenty-one different metals, including Be, Fe, Zr, Mo and W. Finally, we establish a statistical law defining the population of defect cluster sizes produced in an entire cascade event, spanning a broad range of cases from the formation of a single molten zone at a sub-threshold energy to cascade fragmentation at a higher energy. Our analysis explains the increase of the effective power law exponent observed in recent experiments by Yi *et al.* [2], and shows that populations of defects produced by fragmented cascades contain greater numbers of individual Frenkel pairs and small defect clusters, whereas the non-fragmented cascades generate a greater proportion of large defect clusters and dislocation loops.

Cascade fragmentation. – A Monte Carlo BCA model for atomic collisions implemented in SDTrimSP code [26, 27] is used for simulating cascade evolution at high impact energies. The slowing down of atoms is modeled, without giving any consideration to the crystal structure, by a series of random collisions and continuous interaction with electrons. The only input parameters describing the target material are its atomic number and density. The slowing down of knock-on atoms and development of the cascade itself is modeled assuming that moving atoms do not interact. The model uses several rules to describe collisions between the incident atoms and atoms in the material. When both the projectile and the target atom emerge from a collision with their kinetic energies higher than the threshold displacement energy E_d, a vacant site is created. If only the kinetic energy of the projectile is higher than E_d, the target atom moves but stays close to its initial position. When only the kinetic energy of the target atom is higher than E_d, the collision is treated as a replacement event. In the simulations described below, surface effects are not treated, and the term PKA refers to the initial projectile. The model includes two energy loss channels, the kinetic energy transfer in nuclear collisions and electron energy losses.

A BCA model does not treat melting and recrystallization, and hence on its own it cannot describe the structure of cascade debris remaining in the material, or interaction and recombination between radiation defects. To relate BCA simulations to experimental observations, which show the formation of individual sub-cascades [28], we use a sub-domain decomposition method, where we describe the result of cascade evolution in terms of one or several spatially separated molten sub-domains. To perform decomposition, we use information about the amount of energy deposited locally in a certain volume and evaluated using a BCA model calculation, and combine it with the local melting criterion, comparing the density of deposited energy and certain thermodynamic quantities characterizing the material. Initially, a volume large enough to contain the full extent of a cascade is created and divided into elementary cubes. The energy deposited in an EC is calculated by summing the kinetic energy of atoms below a certain cutoff value, comparable to the cohesive energy of the material, and electronic energy losses. We assume that material in a given EC melts if the amount of energy deposited into the EC exceeds

$$E_m = [C(T_m - T) + L]\, V, \tag{1}$$

where C and L are the specific heat and enthalpy of fusion, respectively. T_m and T are the melting temperature and the initial temperature of the material, and V is the volume of the EC. In principle, since the specific heat is a function of temperature, the above equation should involve integration from T to T_m. Also, given the short timescale of a cascade event, melting temperature in a small volume of a cascade is expected to be 15% to 20% higher than the equilibrium melting temperature. Bearing in mind these factors, we treat parameters entering equation (1) as effective quantities, and the equation itself as an estimate, which

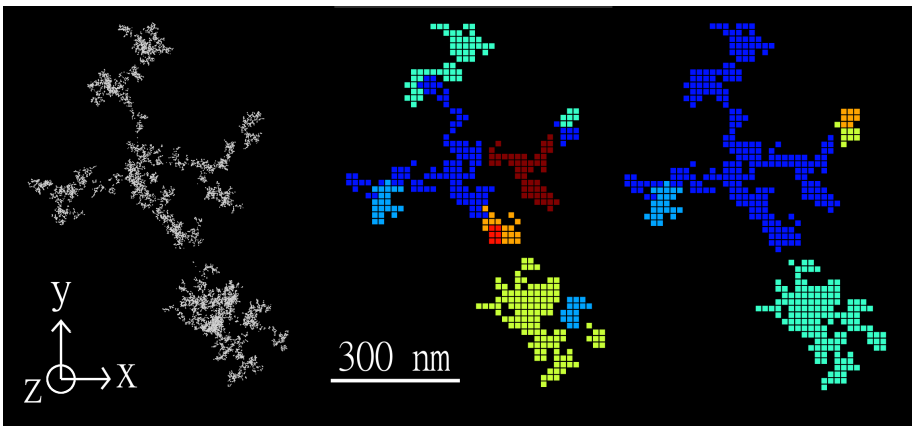

Fig. 1: Left: sketch illustrating a high-energy cascade in tungsten, initiated by a 1 MeV primary knock-on atom, and represented by points where energy was lost in a BCA simulation. Centre: the same cascade represented by a set of cubes, where melting criterion (1) was satisfied. The size of ECs used in the simulation is 15 Å. Right: the same cascade, where electronic losses were added to nuclear losses when applying the melting criterion. All the figures are projections onto the (x, y) plane. The same colour refers to ECs belonging to the same molten sub-domain.

nevertheless is sufficient to provide a suitable numerical input for the model, and is fast and simple to be compatible with a BCA simulation involving analysis of many thousand events. Table 1 gives values evaluated using equation (1) for Be, Fe, Zr, Mo and W, as well as the amount of energy necessary to satisfy the melting criterion in a EC of 10 Å size. W and Mo are able to absorb the largest amount of energy before melting, 77 eV and 66 eV per EC, respectively, because of their high melting temperatures. Zr has the lowest value of E_m because of its low atomic density. Beryllium has a relatively low melting temperature but this is compensated by its high atomic density. In a simulation, after applying the melting

	Z	Specific heat C (J/mol/K)	Melting temperature T_m (K)	Enthalpy of fusion L (kJ/mol)	Atomic Volume (Å^3)	Energy to melt the material (eV)
Be	4	16	1560	8	8.1	37
Al	12	24	923	10.7	16.6	16
Fe	26	25	1811	14	11.9	44
Zr	40	25	2128	21	23.2	30
Mo	42	24	2896	36	15.5	66
W	74	28	3695	35	15.9	77

Table 1: Thermal properties of several representative metals, and the resulting values of E_m computed, using equation (1), for a 10 Å size elementary cube.

criterion to individual ECs, the neighbouring molten areas were merged by considering if any molten regions shared an edge or a corner. These were then treated as parts of a single molten zone. A full set of connected sets of molten ECs forms a sub-domain. To be treated as separate entities, two sub-domains must be isolated from each other by a layer of material that has not melted. Such a layer consists of ECs where no collisions occurred, or where the density of deposited energy is insufficient to cause melting. Once this procedure has been applied, a cascade can be described as consisting of one or several sub-domains, constructed of individual ECs. The left panel of Figure 1 shows a cascade that formed as a result of

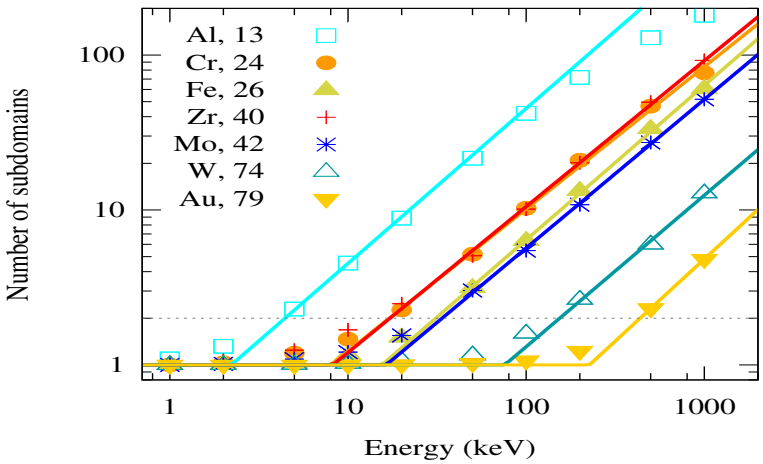

Fig. 2: The number of cascade sub-domains in various metals computed using the domain decomposition method described in the text and plotted as a function of the PKA energy. Lines are fits to simulation data, given by equation $\nu = 1$ if $E \leq 2^{-1/P} E_{fr}$ and $\nu = 2(E/E_{fr})^P$ if $E \geq 2^{-1/P} E_{fr}$, where ν is the number of sub-domains, E_{fr} is the cascade threshold fragmentation energy, above which cascades start splitting into sub-cascades, and the fragmentation exponent P varies in the interval from 0.8 to 1.2.

impact of an 1 MeV PKA in W. The central panel in Figure 1 shows the same cascade, now analyzed using the domain decomposition procedure, where only nuclear losses were included in a calculation of energy deposited into the material. The size of ECs was 15 Å. The right panel in Figure 1 illustrates the case where both nuclear and electron energy losses were included when evaluating the deposited energy. The central panel in Figure 1 shows 15 distinct molten sub-domains, whereas we find only 5 separate sub-domains in the right panel. The difference is caused by the narrow connecting molten "tubes" formed due to electron energy losses occurring along the trajectories of fast moving particles. In what follows, we use only the nuclear energy losses criterion to identify the molten sub-domains.

Figure 2 shows the average number of sub-domains generated by PKAs of various energies in different metals. For clarity, only data for seven out of the twenty-one metals are reproduced here. In all the cases we observe a transition from a single molten domain to a large number of sub-domains occurring at a characteristic threshold energy. The total number of sub-domains ν as a function of PKA energy E is well described by equation $\nu = 1$ if $E \leq 2^{-1/P} E_{fr}$ and $\nu = 2(E/E_{fr})^P$ if $E \geq 2^{-1/P} E_{fr}$, where E_{fr} is the threshold cascade fragmentation energy, and the fragmentation exponent P varies in the interval from 0.8 and 1.2. Cascade fragmentation transitions occur in the interval of PKA energies from 2 keV to 500 keV, depending on the material.

To validate equation (1), we compare the size of molten *volumes* of cascades predicted by MD simulations, with values derived from the BCA model. BCA cascade simulations were performed over a broad interval of PKA energies spanning the range from 1 keV to 10 MeV in W and Fe. It proved necessary to simulate about 1500 cascades per energy to achieve reasonably good statistics. Sub-domain decomposition analysis was then carried out using ECs of 10 or 15 Å. Average molten volumes were compared to MD cascade results over the interval of energies accessible to MD simulations. Figure 3 shows the total volume of cascade molten zones plotted as a function of PKA energy. We find that volumes of molten zones are proportional to PKA energies, with cascades in tungsten being more compact than those in iron. The most significant conclusion that we are able to derive from the data shown in Figure 3 is that over a broad range of PKA energies the BCA sub-domain decomposition model predicts the same molten volumes of collision cascades as MD simulations. We now

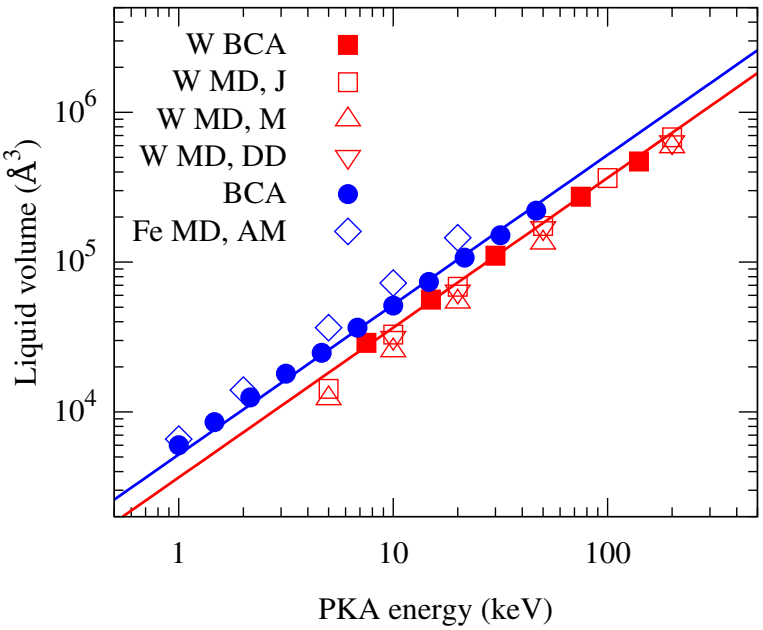

Fig. 3: Comparison of molten volumes of cascades in Fe and W predicted by BCA and MD simulations for various PKA energies. Simulations show that the total volume $V(E)$ of molten material is nearly proportional to the PKA energy. Lines are linear fits of the form $V(E) = V_{fr} \cdot (E/E_{fr})$, where V_{fr} is the volume of the cascade at the fragmentation threshold PKA energy.

proceed to the analysis of statistics of *sizes* of molten sub-domains produced by PKAs with energies below and above the cascade fragmentation energy. The rationale for performing this analysis is based on the fact that, according to Figure 3, it is possible to establish a unique correspondence between the volume of a molten sub-domain and the energy of an effective secondary knock-on atom (SKA) that produces it. Using this correspondence, and also information about the statistics of defect production characterizing individual relatively small cascades [1,2], we are able to derive a statistical law for defect cluster sizes, describing not only individual relatively low-energy cascades but also high-energy cascades undergoing fragmentation.

Figure 4 shows the frequency of occurrence of sub-domains of a given volume in tungsten and iron, plotted as a function of PKA energy. At PKA energies below the cascade fragmentation threshold, the distribution of sub-domain sizes can be well approximated by a delta-function at the PKA energy, accompanied by a relatively low intensity tail of smaller sub-cascades. The form of this distribution reflects the fact that at relatively low sub-threshold PKA energies, in the majority of cases simulations produce only a single molten zone. The fact that we are able to establish a unique correspondence between PKA energies and molten domain volumes, which is illustrated in Figure 3, implies that the occurrence of a sub-cascade splitting energy threshold also necessarily requires that there exists an upper limit on the size of a molten domain. Indeed, cascade fragmentation occurs once the PKA energy exceeds a sub-cascade fragmentation threshold E_{fr}. This takes place at a critical PKA energy or, equivalently, at a critical cascade size. Hence the spectrum of sub-domain volumes shown in Figure 4 can be mapped onto a spectrum of effective SKA energies, where each effective SKA produces a sub-domain of a given size.

In the sub-threshold interval of PKA energies, described by the data shown in Figure 3 for tungsten, it is possible to establish a link between a PKA energy value E and a

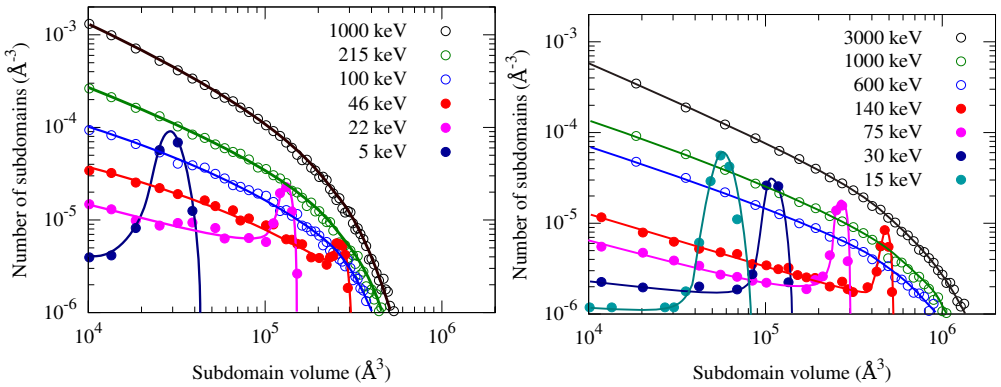

Fig. 4: Distributions of sub-domain volumes in iron (left) and tungsten (right) shown as functions of the PKA energy. The distributions are derived from a BCA study involving 1500 cascade simulations performed for every PKA energy.

distribution $F(n, E)$ of defect cluster sizes generated by such a PKA [1,2]:

$$E \to F(n, E) = A(E)/n^S, \quad n < n^*(E), \tag{2}$$

where for tungsten $S \approx 1.63 < 2$, and $A(E)$ is defined by the normalization condition on the total number of defects produced by a cascade [11, 12]. The fact that the defect size distribution (2) has an upper limit $n^*(E)$ is a mere consequence of the fact that the number of individual defects in a cluster cannot be larger than what can be accommodated inside a molten zone of a finite spatial extend. Assuming that defect clusters produced in cascades are dislocation loops with planar geometry, we find that the upper limit on the number of defects in a cluster is proportional to the projected area of a molten zone, which in the sub-threshold energy range $E < E_{fr}$ varies as $n^*(E) \sim E^{2/3}$. The size of the largest defect cluster n_{fr} that can be produced in a cascade of *any* energy is constrained by the cascade fragmentation transition $n^*(E) < n_{fr} = n^*(E_{fr})$. Values of cascade fragmentation energy E_{fr}, the corresponding molten zone volume V_{fr}, and the maximum number of defects in a cluster n_{fr} are given in Table 2.

	Cascade fragmentation energy E_{fr} (keV)	Fragmentation exponent P	Molten volume V_{fr} (10^3Å^3)	Crystal structure	Lattice constant a (Å)	Burgers vector **b**	Number of defects in a largest cluster n_{fr}
Al	3	0.85	82	FCC	4.05	$\frac{1}{2}\langle 110\rangle$	490
Fe	31	0.99	195	BCC	2.87	$\frac{1}{2}\langle 111\rangle$	530
Zr	17	0.94	180	HCP	3.232	$\frac{1}{3}\langle 11\bar{2}0\rangle$	870
Mo	34	0.9	157	BCC	3.15	$\frac{1}{2}\langle 111\rangle$	630
W	160	1.00	580	BCC	3.17	$\frac{1}{2}\langle 111\rangle$	1450
Au	436	1.06	248	FCC	4.08	$\frac{1}{2}\langle 110\rangle$	4640

Table 2: Values of parameters characterizing cascade fragmentation transitions in various metals.

We now proceed to establish a law of defect clustering valid over a broad range of cascade energies, both below and above the cascade fragmentation transition. Figure 4 shows that

it is possible to establish a correspondence between the energy of a PKA initiating the cascade, and the distribution of sizes, and hence energies, of cascade sub-domains that it generates. By integrating such a distribution $D(\epsilon, E)$ over the energy ϵ of individual sub-domains, we find the total number of sub-domains $\nu(E) = \int_0^E D(\epsilon, E)d\epsilon$, which is the quantity shown in Figure 2. At energies well below the cascade threshold fragmentation energy we can approximate the sub-domain energy distribution by a single value, $D(\epsilon, E) = \delta(\epsilon - E)$, arriving at $\nu(E) = 1$. At energies close to, or above, the cascade fragmentation transition, the distribution of sub-domain energies is a continuous function of ϵ, spanning the entire interval from zero up to E_{fr}. Now the total number of sub-domains shown in Figure 2 is given by $\nu(E) = \int_0^{E_{fr}} D(\epsilon, E)d\epsilon$, $E > E_{fr}$. For PKA energy above the fragmentation threshold energy, the distributions resemble power laws, with a sharp cut-off at the fragmentation energy. The slope of the curves increases slightly as a function of E, showing that at higher energies there appear more smaller sub-domains as opposed to larger ones. Fits to the tungsten data using the functional form $D_V(V, E) \sim (V_{fr}/V)^{Q(E)}$ for $V < V_{fr}$ and $E > E_{fr}$ give exponents $Q(E)$ that increase from 0.68 for $E = 300$ keV PKAs to 0.93 for $E = 3000$ keV PKAs. The distribution of defect cluster sizes for $E > E_{fr}$ can now be evaluated as

$$G(n, E) = \int_0^{E_{fr}} F(n, \epsilon)D(\epsilon, E)d\epsilon, \tag{3}$$

where $F(n, \epsilon)$ is given by equation (2), and where because of the proportionality between V and ϵ we have $D(\epsilon, E) = (V_{fr}/E_{fr})D_V(\epsilon V_{fr}/E_{fr}, E) \sim (E_{fr}/\epsilon)^{Q(E)}$. Using the normalization condition on the total number of sub-domains $\nu(E)$, and the fact that $Q(E) < 1$, we find that for $E > E_{fr}$ the distribution of sub-domains over energies is

$$D(\epsilon, E) = \nu(E)\frac{1 - Q(E)}{E_{fr}}\left(\frac{E_{fr}}{\epsilon}\right)^{Q(E)}, \tag{4}$$

where $\epsilon < E_{fr}$.

To assess the effect of sub-cascade fragmentation on the statistics of defect clustering at PKA energies exceeding the fragmentation transition threshold, we integrated equation (3) numerically, and also used an approximate formula where the dependence of parameter $A(E)$ in equation (2) on the PKA energy was evaluated from the Norgett *et al.* model [11], resulting in

$$A(\epsilon) = A_{fr}\left(\frac{\epsilon}{E_{fr}}\right)^{\frac{2S-1}{3}}.$$

Noting that in (3) the lower limit of integration is defined by the condition that defect clusters of a certain size n form only if the energy of a sub-cascade ϵ exceeds $(n/n_{fr})^{3/2}E_{fr}$, we arrive at

$$G(n, E) \sim n^{-S}\left[1 - \left(\frac{n}{n_{fr}}\right)^{1+S-\frac{3}{2}Q(E)}\right], \quad E > E_{fr}, \tag{5}$$

where the second term in square brackets describes the effect of cascade fragmentation on the statistics of defect clustering. The magnitude of exponent $1 + S - (3/2)Q(E)$ varies from 1.61 for $E = 300$ keV to 1.23 for $E = 3000$ keV. The factor in square brackets in equation (5) vanishes when the defect size n approaches n_{fr}, see Figure 5. This effect is more pronounced in the limit of high PKA energies.

Figure 6 shows distributions of defect cluster sizes in tungsten, produced by PKAs with energies below and above the cascade fragmentation transition, computed assuming $A_{fr} = 2$. We observe that while the maximum size of defect clusters, treated as a function

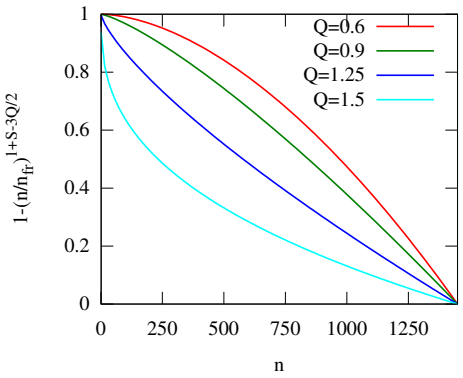

Fig. 5: Factor in square brackets in equation (5) plotted as a function of n for several values of $Q(E)$, with $n_{fr} = 1450$ and $S = 1.63$.

of PKA energy E, increases up to the energy fragmentation threshold, it then remains largely independent of E. The shape of the defect cluster size distribution as a function of E exhibits a systematic trend, giving greater weight to smaller size defect clusters in cascades produced by higher-energy PKAs. Defect cluster size distributions calculated using equation (5) are broadly similar and do not show the presence of defect cluster sizes larger than n_{fr}. Equation (5) and Figure 5 show that cascade fragmentation suppresses the formation of large defect clusters, and favors the generation of smaller clusters and individual point defects. This finding, which is a mere consequence of the functional forms of the defect cluster scaling law (2) and the sub-domain energy distribution $D(\epsilon, E)$ shown in Fig. 4, appears consistent with MD simulations of very high energy cascades [24] where defect populations are visibly dominated by individual defects and small defect clusters. It also agrees with the detailed analysis of defect cluster size frequency distributions derived from experimental observations of 400 keV cascades in tungsten [29].

While at this point we feel that it would be premature to attempt to identify, at a reasonable level of confidence, the functional form of a global scaling law of defect clustering suitable for all the elements in the Periodic table, it appears that the defect cluster size scaling law given by equation (5) and illustrated in Fig. 6 interpolates the data well and may be suitable for practical calculations.

It does not escape our attention that distributions of defect cluster sizes generated by high-energy fragmented cascades are broadly similar to the distributions characterizing relatively low energy near-threshold cascade events. This points out to the possible universality of defect cluster size distributions produced in collision cascades initiated by PKAs with energies varying over a fairly broad energy interval.

* * *

This work was part-funded by the RCUK Energy Programme [grant number EP/I501045]. This work has been carried out within the framework of the EUROfusion Consortium and has received funding from the Euratom research and training programme 2014-2018 under grant agreement No 633053. The views and opinions expressed herein do not necessarily reflect those of the European Commission. The work was also supported by CEA/DEN under RSTB/MATIX research program, and by the Enabling Research project TriCEM on Tritium Retention in Controlled and Evolving Microstructure.

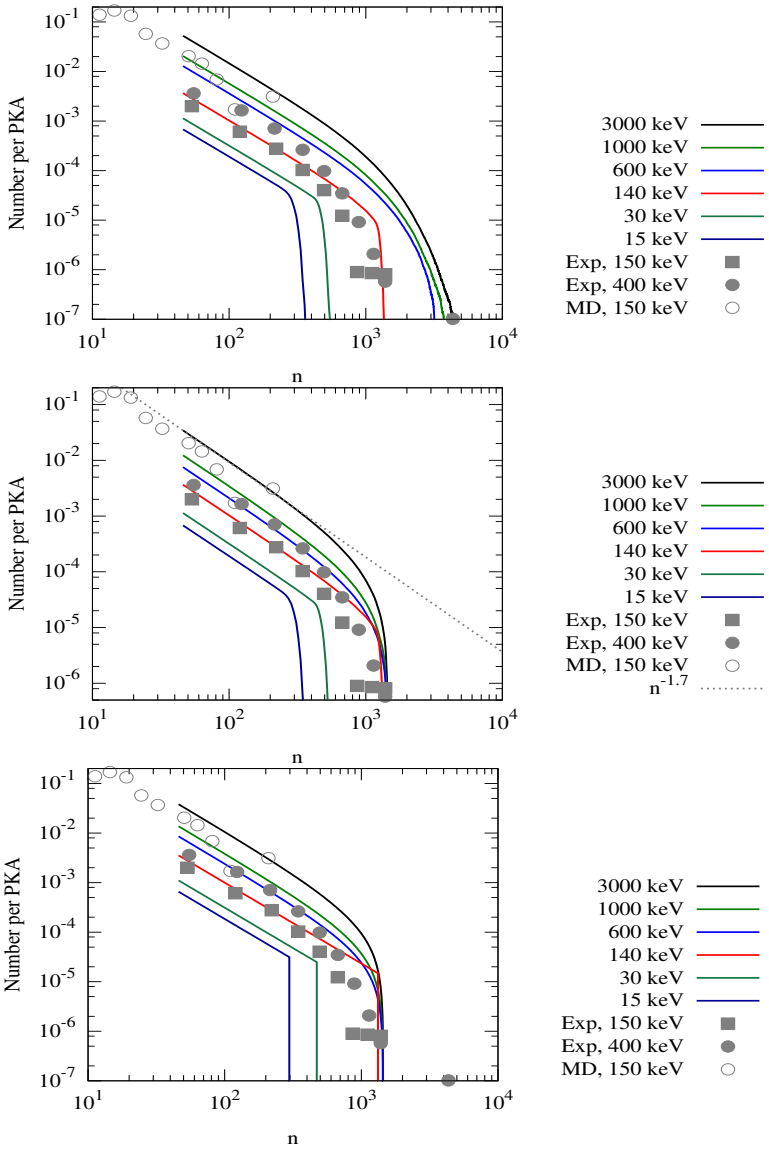

Fig. 6: Distributions of defect cluster sizes in tungsten, produced by PKAs with various energies. Data points are results of MD simulations [1] and experimental electron microscope observations of defect clusters [2]. The slope of the curve at low PKA energies is close to = 1.63. The slope increases slightly increases to 1.7 for $E = 3000$ keV. Top panel is computed using numerical integration of equation (3) and includes domains with sizes exceeding the fragmentation size, resulting from overlap between cascade branches. Panel in the centre excludes this part of defect size distribution. Bottom panel shows the curves given by analytical expression (5) with exponents fitted to the BCA data.

REFERENCES

[1] A.E. Sand, S.L. Dudarev, and K. Nordlund, High-energy collision cascades in tungsten: Dislocation loops structure and clustering scaling laws, *EPL*, **103** (2013) 46003.

[2] X. Yi, A.E. Sand, D.R. Mason, M.A. Kirk, S.G. Roberts, K. Nordlund and S.L. Dudarev, Direct observation of size scaling and elastic interaction between nano-scale defects in collision cascades, *EPL*, **110** (2015) 36001.

[3] M.R. Gilbert, and J.-Ch. Sublet, Neutron-induced transmutation effects in W and W-alloys

in a fusion environment. *Nucl. Fusion* **51** (2011) 043005.
[4] C.S. Becquart and C. Domain, Migration energy of He in W revisited by *ab initio* calculations, *Phys. Rev. Lett.*, **97** (2006) 196402.
[5] J. Boisse, C. Domain, C.S. Becquart, Modelling self trapping and trap mutation in tungsten using DFT and Molecular Dynamics with an empirical potential based on DFT, *Journal of Nuclear Materials*, **455** (2014) 10.
[6] L. Sandoval, D. Perez, B.P. Uberuaga, and A.F. Voter, Competing kinetics and He bubble morphology in W, *Phys. Rev. Lett.*, **114** (2015) 105502.
[7] C.D. Hardie, C.A. Williams, S. Xu, S.G. Roberts, Effects of irradiation temperature and dose rate on the mechanical properties of self-ion implanted Fe and Fe-Cr alloys, *Journal of Nuclear Materials* **439** (2013) 33.
[8] A. Xu, C. Beck, D.E.J. Armstrong, K. Rajan, G.D.W. Smith, P.A.J. Bagot, and S.G. Roberts, Ion-irradiation-induced clustering in W-Re and W-Re-Os alloys: A comparative study using atom probe tomography and nanoindentation measurements, *Acta Materialia* **87** (2015) 121.
[9] M.R. Gilbert, S.L. Dudarev, S. Zheng, L.W. Packer and J.-Ch. Sublet, An integrated model for materials in a fusion power plant: transmutation, gas production, and helium embrittlement under neutron irradiation. *Nucl. Fusion* **52** (2012) 083019.
[10] L. Zhang, C.-C. Fu, and G.-H. Lu, Energetic landscape and diffusion of He in α-Fe grain boundaries from first principles, Phys. Rev. B **87** (2013) 134107; L. Zhang, C.-C. Fu E. Hayward, G.-H. Lu, Properties of He clustering in α-Fe grain boundaries, *Journal of Nuclear Materials*, **459** (2015) 247.
[11] M. J. Norgett, M. T. Robinson, I.M. Torrens, A proposed method of calculating displacement dose rates, *Nucl. Eng. Design* **33** (1975) 50.
[12] R. Stoller, Primary Radiation Damage Formation, in: Comprehensive Nuclear Materials, Ed. R.J.M. Konings, Elsevier, Amsterdam, 2012.
[13] T. Diaz de la Rubia and M. W. Guinan, New Mechanism of Defect Production in Metals: A Molecular-Dynamics Study of Interstitial-Dislocation-Loop Formation in High-Energy Displacement Cascades, *Phys. Rev. Lett.*, **66** (1991) 2766.
[14] C. H. Woo and B. N. Singh, Production bias due to clustering of point defects in irradiation-induced cascades, *Philosophical Magazine A* **65** (1992) 889.
[15] L. Oddershede, P. Dimon, and J. Bohr, Self-organized criticality in fragmenting. *Phys. Rev. Lett.*, **71** (1993) 3107.
[16] M. R. Gilbert, J. Marian, J.-Ch. Sublet, Energy spectra of primary knock-on atoms under neutron irradiation, *Journal of Nuclear Materials*, **467** (2015) 121.
[17] R. Stoller, Subcascade formation in displacement cascade simulations: Implications for fusion reactor materials, *Journal of Nuclear Materials*, **271 & 272** (1999) 57.
[18] M. Hou, Fuzzy clustering methods: an application to atomic displacement cascades in solids, *Phys. Rev. A* **39** (1989) 2817.
[19] Y. Satoh, S. Kojima, T. Yoshiie, M. Kiritani, Criterion of subcascade formation in metals from atomic collision calculation. *Journal of Nuclear Materials*, **179** (1991) 901.
[20] D. Simeone, L. Luneville, and Y. Serrys, Cascade fragmentation under ion beam irradiation: a fractal approach. *Phys. Rev. E* **82** (2010) 011122.
[21] L. Luneville, D. Simeone, and W. J. Weber, Study of the fragmentation of a displacement cascade into subcascades within the Binary Collision Approximation framework, *Journal of Nuclear Materials*, **415** (2011) 55.
[22] Y. T. Cheng, M. A. Nicolet, W. L. Johnson, From cascade to spike - a fractal geometry approach, *Phys. Rev. Lett.* **58** (1987) 2083.
[23] H. L. Heinisch and B. N. Singh, On the structure of irradiation-induced collision cascades in metals as a function of recoil energy and crystal structure, *Philos. Mag. A*, **67** (1993) 407.
[24] E. Zarkadoula, S. L. Daraszewicz, D. M. Duffy, M. A. Seaton, I. T. Todorov, K. Nordlund, M. T. Dove and K. Trachenko, The nature of high-energy radiation damage in iron, *J. Phys.: Condens. Matter* **25** (2013) 125402.
[25] C. H. M. Broeders and A. Y. Konobeyev, Displacement cross-sections for tantalum and tungsten irradiated with protons at energies up to 1 GeV, *Journal of Nuclear Materials*, **336** (2005) 201; C. H. M. Broeders, A. Y. Konobeyev and C. Villagrasa, Neutron displacement cross-sections for tantalum and tungsten at energies up to 1 GeV, *Journal of Nuclear Materials*, **342** (2005) 68.

[26] W. Eckstein, Computer Simulation of Ion-Solid Interactions, (Springer, Berlin, 1991).
[27] A. Mutzke, R. Schneider, W. Eckstein and R. Dohmen, SDTrimSP version 5.00, IPP Report 12/08, Max-Planck-Institut für Plasmaphysik (2011)
[28] M. L. Jenkins and M. A. Kirk, Characterization of radiation damage by transmission electron microscopy, (Institute of Physics, Bristol, 2001), pp. 145–158.
[29] D. R. Mason and X. Yi (2015), unpublished.